(This is a sample cover image for this issue. The actual cover is not yet available at this time.)

Quaternary Science Reviews 59 (2013) 101–111

Contents lists available at SciVerse ScienceDirect

Quaternary Science Reviews

journal homepage: www.elsevier.com/locate/quascirev

Exposure-age record of Holocene ice sheet and ice shelf change in the northeast Antarctic Peninsula

Greg Balco [a,*], Joerg M. Schaefer [b], LARISSA group [1]

[a] Berkeley Geochronology Center, 2455 Ridge Road, Berkeley, CA 94709, USA
[b] Lamont-Doherty Earth Observatory of Columbia University, 61 Route 9W, Palisades, NY 10964, USA

ARTICLE INFO

Article history:
Received 13 March 2012
Received in revised form
12 October 2012
Accepted 18 October 2012
Available online

Keywords:
Larsen Ice Shelf
Weddell Sea
Deglaciation
Antarctic Peninsula
Cosmogenic-nuclide geochronology
Exposure dating

ABSTRACT

This paper describes glacial–geologic observations and cosmogenic-nuclide exposure ages from ice-free areas adjacent to the Sjögren, Boydell, and Drygalski Glaciers of the northeast Antarctic Peninsula. These provide a record of Holocene glacier and ice shelf change in this region. Early Holocene ice surface elevation near the present coastline was locally at least 500 m above present sea level, but our observations do not constrain the maximum thickness of Last Glacial Maximum (LGM) ice or the time at which it was attained. The boundary between frozen-based and wet-based ice reached a maximum elevation of 100–150 m above present sea level. The ice surface elevation decreased from 300–500 m elevation to near present sea level between 9 ka and ca 4 ka. Below 160 m elevation, we observed a bimodal distribution of apparent exposure ages in which a population of glacially transported clasts with mid-Holocene exposure ages coexists with another that has exposure ages of 100–600 years. We consider the most likely explanation for this to be i) complete deglaciation of currently ice-free areas, which presumably required the absence of ice shelves, at 3.5–4.5 ka, followed by ii) subsequent ice shelf formation and grounding line advance after ca 1.4 ka, and iii) complete re-exposure of the sites after ice shelf breakup and glacier surface lowering in recent decades. This explanation is consistent with marine sedimentary records indicating that ice shelves in the Prince Gustav Channel and Larsen A embayment were absent in the middle to late Holocene and were re-established within the last 2000 years.

1. Introduction

This paper describes glacial–geologic observations and cosmogenic nuclide exposure ages from terrestrial sites on the east side of the northern Antarctic Peninsula (Fig. 1). Glacier change in this region during the past several decades has been notable for the rapid and spectacular collapse of major ice shelves, mainly i) the ice shelves occupying the southern end of Prince Gustav Channel (PGC), Larsen Inlet, and the Larsen A embayment, in 1995; and ii) the majority of the Larsen B ice shelf in 2002 (for summaries, see Rott et al., 1996; Vaughan and Doake, 1996; Scambos et al., 2004; Cook and Vaughan, 2010). These ice shelf collapses resulted in extremely rapid (over a period of a few years) drawdown and grounding line retreat of glaciers feeding these ice shelves. Marine-geological evidence (Pudsey and Evans, 2001; Brachfeld et al., 2003; Domack et al., 2005) indicates that the PGC–Larsen A ice shelf system disappeared and reformed at least once during the Holocene, but the Larsen B ice shelf was present throughout the Holocene. This paper describes geologic and geochronologic evidence from ice-free sites on land adjacent to glaciers that fed the former PGC–Larsen A ice shelf system. This complements marine records of glacier and ice shelf changes by providing an independent chronology for these changes and by providing information about past changes in ice thickness as well as extent.

2. Review of LGM-to-Holocene ice sheet change, northeast Antarctic Peninsula

Recent reviews of glacier change in the northeast Antarctic Peninsula between the Last Glacial Maximum (LGM) and the present include Davies et al. (2012), Johnson et al. (2011), Heroy and Anderson (2007), Domack et al. (2005), and Evans et al. (2005); the brief summary in the remainder of this section is drawn from these references. We use the term "Last Glacial Maximum" loosely to

* Corresponding author. Tel.: +1 510 644 9200; fax: +1 510 644 9201.
E-mail address: balcs@bgc.org (G. Balco).

[1] The LARISSA ("Larsen Ice Shelf System, Antarctica") group includes G. Balco, S. Brachfeld, M. de Batist, E. Domack, A. Gordon, T. Haran, J.-P. Henriet, B. Huber, S. Ishman, S. Jeong, M. King, C. Lavoie, A. Leventer, M. McCormick, E. Mosley-Thompson, E. Pettit, T. Scambos, C. Smith, L. Thompson, M. Truffer, C. van Dover, M. Vernet, J. Wellner, K. Yu, and V. Zagorodnov.

0277-3791/$ – see front matter © 2012 Elsevier Ltd. All rights reserved.
http://dx.doi.org/10.1016/j.quascirev.2012.10.022

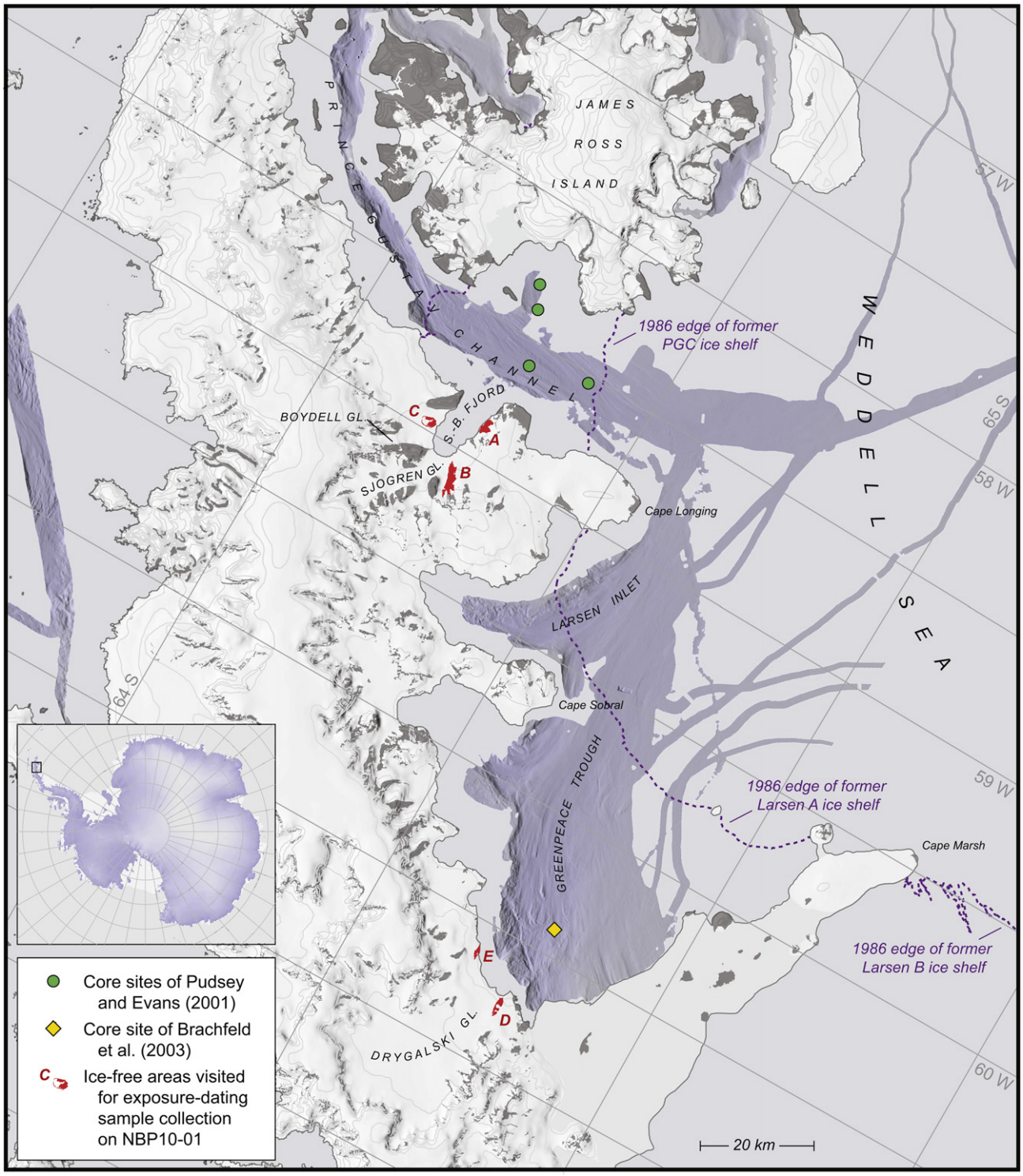

Fig. 1. East coast of the Antarctic Peninsula between Cape Marsh and James Ross Island. Inset map of Antarctica shows location. All vector data, including former ice shelf edges, are from the SCAR Antarctic Digital Database (https://www.add.scar.org). Shaded-relief topography of land areas is generated from the RAMP DEM (Liu et al., 2001). The blue shaded area shows shaded-relief bathymetry generated from selected multibeam swath data compiled by Johnson et al. (2011). The streamlining evident on the seafloor records past ice flow directions that presumably reflect the ice sheet configuration during the LGM and/or subsequent deglaciation. Red areas highlight ice-free areas where we collected exposure-dating samples surrounding the Sjögren–Boydell fjord (sites A–C) and near the grounding line of the Drygalski Glacier (sites D and E). We only show marine sediment cores that we specifically discuss in the text; many others have been collected from this region. (For interpretation of the references to color in this figure legend, the reader is referred to the web version of this article.)

refer to the period of the Last Glacial–Interglacial cycle during which the Antarctic ice sheets were near their maximum geographic extents, between approximately 25–15 ka (all ages in this paper are stated in calendar years before present). Multibeam bathymetric surveys of the seafloor to the northeast of the Peninsula show evidence that grounded ice extended nearly to the edge of the Weddell Sea continental shelf (past the eastern edge of Fig. 1) during the most recent glacial cycle, and this is generally agreed to

represent the maximum extent of grounded ice at the LGM. Ice flow directions inferred from streamlined seafloor features show that flow of Peninsula-derived ice was concentrated in ice streams occupying prominent topographic lows: ice from the eastern Peninsula west of James Ross Island (JRI) flowed around JRI in the northern and southern branches of PGC; ice from the southern limb of PGC joined eastward-flowing ice from Larsen Inlet and the Larsen A embayment to form an ice stream south of JRI; and ice from the Larsen B embayment most likely flowed into a separate ice stream south of Cape Marsh. The fact that Peninsula-derived erratics of Pleistocene age are only found at low elevations on JRI indicates that JRI formed a distinct ice dome and was not overridden by Peninsula ice during Pleistocene glacial maxima.

Glaciomarine sediments on the continental shelf east and south of JRI include significant amounts of recycled detrital carbon, so marine sediment cores from this region have core-top radiocarbon ages that exceed the marine reservoir age by thousands of years. Thus, radiocarbon dates for ice recession from these sites are subject to large and uncertain corrections for this effect. Nonetheless, they appear to indicate that the grounding line retreated from the shelf edge by approximately 18.5 ka; that the southern end of PGC was free of grounded ice by approximately 13–11 ka; and that retreat of grounded ice from the majority of PGC took place between 10.5 ka and 6.2 ka. Brachfeld et al. (2003) used geomagnetic paleointensity dating of a sediment core (Fig. 1) in the Greenpeace Trough, Larsen A embayment, to show that grounded ice was absent at this site by 10.7 ka. Several grounding line positions can be identified from multibeam and seismic data on the continental shelf within and east of the Larsen A embayment, implying that retreat of the ice margin was unsteady and punctuated by stillstands of unknown duration. To summarize, the marine deglaciation chronology indicates that grounding line retreat from the outer continental shelf began before 18.5 ka, the rate of retreat may have been highly variable, and grounding line positions approached the present coastline in at least some locations by ca 10 ka.

Marine sedimentary records also show that after grounding line retreat was complete, much of the inner continental shelf remained covered by ice shelves, but ice shelves in PGC and the Larsen A embayment broke up and reformed at least once during the Holocene. Brachfeld et al. (2003) used data from a core in the Greenpeace Trough (Fig. 1) to show that the Larsen A ice shelf was absent one or more times between 1.4 and 3.8 ka. Pudsey and Evans (2001) used data from cores in southern PGC (Fig. 1) to show that the PGC ice shelf was absent approximately 2–5 ka. These two age estimates are indistinguishable given their uncertainties. Domack et al. (2005), on the other hand, showed that the Larsen B ice shelf was present throughout the Holocene.

Primarily because of the difficulty of access to terrestrial sites on the Peninsula itself, which are mostly defended by heavily crevassed and fast-moving glaciers, existing terrestrial age constraints in this region come from the large and relatively accessible coastal ice-free areas on JRI and nearby islands. Johnson et al. (2011) obtained 16 cosmogenic-nuclide exposure ages on Peninsula-derived erratics found at relatively low elevation at four sites on JRI and Seymour Island. Sites most distal to the central plateau of JRI, which most likely record the disappearance of the Peninsula-derived ice streams occupying major troughs, showed minimum exposure ages near 8 ka; sites on JRI itself closer to the central plateau, which presumably record subsequent shrinkage of outlet glaciers to the JRI ice cap, showed minimum exposure ages near 6.5 ka. Ingolfsson et al. (1992), Hjort et al. (1997, 1998), and Strelin et al. (2006) obtained radiocarbon dates from terrestrial sites on JRI that provide minimum ages for retreat of Peninsula ice from PGC and internal fjords and bays of JRI, as well as some age constraints on subsequent changes of JRI-sourced glaciers. Strelin et al. (2006) concluded from these data that ice-free areas emerged, presumably upon retreat of the PGC ice stream, by 10.7–8.4 ka. Also, they defined six Holocene advances of JRI-sourced glaciers: at 7.6–7.4 ka, 5.6–5 ka, and shortly after 4.4 ka; and three bracketed between 4.4 ka and ca 400 years ago. To summarize, the terrestrial observations are consistent with the marine chronology for grounding line retreat to near the present coastline by ca 10 ka, and provide additional information about Holocene glacier change.

3. Sample collection and analytical methods

3.1. Helicopter operations on NBP10-01

A recent cruise of the research icebreaker *Nathaniel B. Palmer* in 2010 (NBP10-01) formed the main field deployment for the "LARISSA" (LARsen Ice Shelf System, Antarctica) project. An unusual aspect of this cruise was that the *Palmer* carried two helicopters, which allowed us to make glacial–geological observations and collect exposure-dating samples at ice-free sites on the eastern edge of the Peninsula itself that would be impossible to reach by any other means. Limits on ship positioning imposed by sea ice conditions and limits on helicopter operations imposed by weather both restricted the amount of time available for this work; we had available a total of 24 h of ground time, at five separate sites, in four days of helicopter operations (Fig. 1). This was sufficient to make basic geological observations and collect a reconnaissance data set of 33 exposure-dating samples.

3.2. Sample collection

Our approach in collecting samples for exposure-dating was similar to that of a number of previous studies that have used this method in Antarctica (e.g., Stone et al., 2003; Sugden et al., 2005; Bentley et al., 2010; Todd et al., 2010). The basis of this approach is that glacially transported clasts quarried from glacier beds have not been exposed to the cosmic ray flux, so contain a negligible cosmogenic-nuclide inventory. Once deposited at a retreating ice margin, they are exposed to the cosmic-ray flux, so their cosmogenic-nuclide exposure age corresponds to the deglaciation age of the site. As in these other studies, we predominantly collected loose surface cobbles, but in two cases we sampled boulders (see Table 1). Our criteria for sample collection were as follows. First, clasts that we sampled are 'glacial erratics,' that is, they showed evidence for glacial transport, including exotic lithology and/or signs of subglacial or englacial transport such as impact marks, faceting, and polishing. Second, clasts were perched upon, rather than embedded in, surficial materials, indicating that they were most likely emplaced directly as a result of ablation of glacier ice and had not been affected by creep or periglacial disturbance. Third, clasts were located in places to which they could not have been delivered by postdepositional rolling or sliding; in most cases this means they were located atop hummocks or local high points rather than at the base of slopes. We found clasts that met these criteria on substrates of bedrock, felsenmeer, and locally derived colluvium. At one site (site "A"; see description below), we also collected several samples of in-place bedrock. As noted in many previous exposure-dating studies in Antarctica (e.g., Sugden et al., 2005), the relative ineffectiveness of subglacial erosion by cold-based glaciers means that apparent exposure ages of recently deglaciated bedrock samples are often much greater than their true deglaciation age. Thus, Antarctic bedrock samples are not expected to provide an accurate deglaciation chronology (except possibly by accident). The purpose of collecting these samples was to obtain

Table 1
^{10}Be exposure ages from LARISSA/NBP10-01.

Sample name	Date collected	Latitude (DD)	Longitude (DD)	Elevation (masl)[a]	Sample type	Lithology	Sample thickness (cm)	Topographic shielding	^{10}Be concentration (atoms g^{-1})[b]	Apparent exposure age (yr)[c,d]
Sjögren/Boydell fjord, site A: Downham Peak										
10-LAR-001-SJO	11-Jan-2010	−64.28117	−58.88529	518	Bedrock	Quartz vein in schist	3	0.9941	231600 ± 5900	26440 ± 680 (970)
10-LAR-002-SJO	11-Jan-2010	−64.27914	−58.88249	406	Bedrock	Quartz vein in schist	2	0.9947	253400 ± 6400	31910 ± 820 (1200)
10-LAR-003-SJO	11-Jan-2010	−64.27712	−58.87878	300	Bedrock	Quartz vein in schist	5	0.9964	207900 ± 4800	29670 ± 700 (1040)
10-LAR-004-SJO	11-Jan-2010	−64.27523	−58.87411	204	Erratic cobble	Granodiorite	7	0.9977	258400 ± 5600	41310 ± 900 (1410)
10-LAR-005-SJO	11-Jan-2010	−64.27219	−58.87606	84	Erratic cobble	Vein quartz	7	0.9977	48000 ± 1100	8600 ± 200 (300)
10-LAR-006-SJO	11-Jan-2010	−64.27219	−58.87606	80	Bedrock	Quartz vein in schist	6	0.9977	33400 ± 1100	5940 ± 200 (250)
Sjögren/Boydell fjord, site B: unnamed nunatak, south side of fjord										
10-LAR-008-SJO	7-Feb-2010	−64.26423	−59.07658	303	Erratic cobble	Granite	5	0.9984	47800 ± 1100	6750 ± 150 (230)
10-LAR-009-SJO	7-Feb-2010	−64.26423	−59.07658	303	Erratic cobble	Granite	5.5	0.9984	50000 ± 1200	7090 ± 160 (250)
10-LAR-010-SJO	7-Feb-2010	−64.26089	−59.06788	258	Erratic cobble	Granite	7	0.9995	139400 ± 3500	20960 ± 530 (760)
10-LAR-011-SJO	7-Feb-2010	−64.26287	−59.07997	285	Erratic cobble	Granite pegmatite	5	0.9986	141400 ± 4700	20390 ± 680 (870)
10-LAR-012-SJO	7-Feb-2010	−64.26629	−59.08132	343	Erratic cobble	Granite	5	0.9988	336000 ± 7100	46060 ± 980 (1560)
10-LAR-013-SJO	7-Feb-2010	−64.26629	−59.08132	343	Erratic cobble	Granite	4.5	0.9988	51000 ± 1400	6900 ± 180 (260)
10-LAR-014-SJO	7-Feb-2010	−64.27373	−59.09754	487	Erratic cobble	Granite	6	0.9979	430700 ± 9100	52000 ± 1100 (1800)
10-LAR-015-SJO	7-Feb-2010	−64.27373	−59.09754	487	Erratic cobble	Granite	6	0.9979	262300 ± 5500	31500 ± 670 (1070)
10-LAR-016-SJO	7-Feb-2010	−64.26757	−59.08307	358	Erratic cobble	Granite	6	0.9995	54600 ± 1200	7370 ± 160 (250)
Sjögren/Boydell fjord, site C: unnamed nunatak near grounding line of Boydell Glacier, north side of fjord										
10-LAR-017-SJO	8-Feb-2010	−64.19531	−58.97953	116	Erratic cobble	Metagreywacke	6	0.9993	29000 ± 850	4970 ± 150 (200)
10-LAR-018-SJO	8-Feb-2010	−64.19531	−58.97953	116	Erratic cobble	Vein quartz	6.5	0.9993	27700 ± 690	4770 ± 120 (170)
10-LAR-019-SJO	8-Feb-2010	−64.19653	−58.97949	97	Erratic cobble	Vein quartz	6	0.9992	1400 ± 240	245 ± 42 (42)
10-LAR-020-SJO	8-Feb-2010	−64.19653	−58.97949	97	Erratic cobble	Metasandstone	4	0.9992	1270 ± 280	218 ± 48 (48)
10-LAR-021-SJO	8-Feb-2010	−64.19726	−58.97807	74	Erratic cobble	Metasandstone	6	0.9988	2000 ± 1200	350 ± 220 (220)
10-LAR-022-SJO	8-Feb-2010	−64.19726	−58.97807	74	Erratic cobble	Vein quartz	5	0.9988	24200 ± 1300	4310 ± 230 (250)
10-LAR-023-SJO	8-Feb-2010	−64.19939	−58.97813	39	Erratic cobble	Metagreywacke	5.5	0.9985	18100 ± 3300	3360 ± 600 (610)
10-LAR-024-SJO	8-Feb-2010	−64.19939	−58.97813	39	Erratic cobble	Vein quartz	8	0.9985	18070 ± 590	3420 ± 110 (140)
Drygalski Glacier, site D: Sentinel Nunatak										
10-LAR-025-DRY	18-Feb-2010	−64.77248	−60.79322	516	Erratic cobble	Vein quartz	4	0.9934	36800 ± 1000	4220 ± 120 (160)
10-LAR-028-DRY	18-Feb-2010	−64.77303	−60.78911	456	Erratic 1.2 m boulder	Granite	7	0.9885	609900 ± 7600	77630 ± 990 (2290)
10-LAR-029-DRY	18-Feb-2010	−64.77295	−60.79028	465	Erratic 2 m boulder	Granite	6	0.9862	76100 ± 1700	9380 ± 210 (320)
Drygalski Glacier, site E: unnamed nunatak near north side of calving margin										
10-LAR-030-DRY	18-Feb-2010	−64.70287	−60.62598	49	Erratic cobble	Vein quartz	5	0.9844	3410 ± 330	632 ± 60 (62)
10-LAR-031-DRY	18-Feb-2010	−64.70287	−60.62598	50	Erratic cobble	Vein quartz	5.5	0.9844	3250 ± 350	605 ± 65 (67)
10-LAR-032-DRY	18-Feb-2010	−64.70238	−60.62435	84	Erratic cobble	Granodiorite	3	0.9973	700 ± 250	122 ± 44 (44)
10-LAR-033-DRY	18-Feb-2010	−64.70172	−60.61989	101	Erratic cobble	Granodiorite	5.5	0.9949	35600 ± 1200	6210 ± 200 (260)
10-LAR-034-DRY	18-Feb-2010	−64.70098	−60.61342	133	Erratic cobble	Granite	5.5	0.9979	28200 ± 1400	4750 ± 240 (270)
10-LAR-035-DRY	18-Feb-2010	−64.69998	−60.61063	159	Erratic cobble	Granite	5.5	0.9997	33400 ± 1100	5450 ± 180 (230)
10-LAR-036-DRY	18-Feb-2010	−64.69998	−60.61063	159	Erratic cobble	Granite	5.5	0.9997	620 ± 310	102 ± 51 (51)

[a] Measured by barometer traverse from temporary benchmarks established using Trimble survey GPS system. Estimated uncertainty ±1.5 m.
[b] Normalized to the "07KNSTD" Be isotope ratio standard series. See Nishiizumi et al. (2007).
[c] Exposure ages computed assuming zero erosion and a rock density of 2.65 g cm^{-2}, using the online exposure age calculator of Balco et al. (2008) with the "St" scaling scheme and a new production rate calibration data set constructed from unpublished results of the CRONUS-EARTH project. See text for additional details.
[d] Both internal uncertainties (including measurement uncertainties only) and external uncertainties (also including production rate uncertainties) are shown. Value in parentheses is the external uncertainty. See Balco et al. (2008) for additional details.

some information about bedrock surface erosion rates, and we report the results here for completeness.

3.3. Analytical methods

We extracted quartz from these samples by crushing, sieving to a grain size smaller than the original mineral size, and a combination of heavy liquid separation, magnetic separation, boiling in H_3PO_4, and repeated etching in dilute HF. We extracted Be in the Cosmogenic Nuclide Lab at the Lamont–Doherty Earth Observatory, Columbia University, by standard methods of HF dissolution and column chromatography. Our ^{9}Be carrier solution was derived from deep-mined beryl and has a ^{10}Be/^{9}Be ratio of $2 \pm 3 \times 10^{-16}$. We measured Be isotope ratios at the Center for Accelerator Mass Spectrometry, Lawrence Livermore National Laboratory. Total carrier and process blanks were 9500 ± 3500 atoms ^{10}Be; this was <3% of the total number of atoms present for samples with mid-Holocene and older apparent exposure ages, but 10–50% of the total number of atoms present for very young samples with apparent exposure ages of 100–200 years. ^{10}Be concentrations are normalized to the "07KNSTD" isotope ratio standards of Nishiizumi et al. (2007). We computed exposure ages using the 'St' scaling scheme in the online calculator of Balco et al. (2008), version 2.2, with an unpublished production rate calibration data set recently generated by the CRONUS-Earth project (J. Stone, written communication). This calibration data set and scaling scheme imply a reference ^{10}Be production rate of 4.20 ± 0.20 atoms g^{-1} yr^{-1}; this does not differ significantly from production rates predicted by recent calibration data sets of Balco et al. (2009), Putnam et al. (2010), and Kaplan et al. (2011), and the differences among these would not affect any of our conclusions. Exposure ages described here are apparent exposure ages, meaning that they are computed under the assumption that each sample experienced one period of exposure at the surface without any erosion. Table 1 shows ^{10}Be concentrations and apparent exposure ages.

4. Observations, results, and discussion

4.1. Sjögren–Boydell fjord and the Prince Gustav Channel ice shelf: site details

Before the breakup of the PGC ice shelf in 1995, the Sjögren and Boydell Glaciers flowed together into a single fjord glacier discharging into the ice shelf. After ice shelf disintegration, both glaciers experienced rapid surface lowering and, presumably, grounding line retreat (De Angelis and Skvarca, 2003). They are now distinct glaciers calving into a fully ice-free fjord (Fig. 1; henceforth called the Sjögren–Boydell fjord). We visited three ice-free areas adjacent to this fjord (Figs. 1 and 2): a prominent peak on the south side of the outer fjord named Downham Peak (site "A"); an unnamed bedrock ridge on the south side of the inner fjord near the current calving margin of the Sjögren Glacier (site "B"); and an unnamed small nunatak at low elevation on the north side of the inner fjord near the current calving margin of the Boydell Glacier (site "C").

4.1.1. Downham Peak (site A)

Downham Peak is a pyramidal peak (summit 535 m) atop a lower-angle bedrock bench, at the foot of which is a precipitous slope that falls 80 m to the fjord (Fig. 2). We could not descend below this break in slope. The bottom of the steep slope is overlain by a prominent, fresh, and unweathered moraine, approximately 40 m above present sea level, which presumably records the pre-1995 ice shelf surface elevation. The bedrock is a fissile pelitic schist, and ice-free areas are nearly entirely covered with frost-shattered bedrock outcrop, felsenmeer, or colluvium derived from local bedrock. Frost cracking and poorly developed patterned ground are locally present in colluvium-covered areas. Between 80 m and 240 m elevation, we found sparse evidence of past ice cover, including several erratic clasts and traces of striations on several upstanding bedrock knobs. Near 200 m elevation, a pavement composed of loose clasts of local bedrock displayed striations, on individual clasts, that were directionally concordant across many clasts. We did not observe any evidence of past ice cover above 240 m elevation. At the lowest site we were able to visit (near 80 m elevation), bedrock knobs were coarsely streamlined and striated surfaces were abundant. We interpret these observations as follows. First, the presence of striations and erratics up to 240 m elevation indicates past ice cover at least up to this elevation. Second, the scarcity of striations above 80 m, the presence of concordant striations on loose clasts, and the presence of erratics overlying undisturbed bedrock weathering features all indicate that these areas were covered by ice whose basal temperature was below freezing; this would permit some basal sliding without significant disturbance of the bed (e.g., Cuffey et al., 2000). Third, the boundary between overriding ice that was always frozen to its bed and ice that was wet-based for at least some time lies near 80 m elevation.

Glacially transported clasts are scarce at this site, and we found only two that were suitable for exposure dating. Fig. 3 shows results. First, at the lowest part of this site we could access, streamlined bedrock (80 m) and erratic (84 m) samples had apparent exposure ages of 6 and 8.6 ka, respectively. Similar Holocene ages from both erratics and bedrock imply that subglacial erosion at this site was most likely adequate to remove any pre-LGM cosmogenic-nuclide inventory in the bedrock surface, which is consistent with the geomorphic evidence for significant subglacial erosion at this elevation described above.

At higher elevations at this site, one erratic has an apparent exposure age of 41 ka, and several bedrock samples have apparent

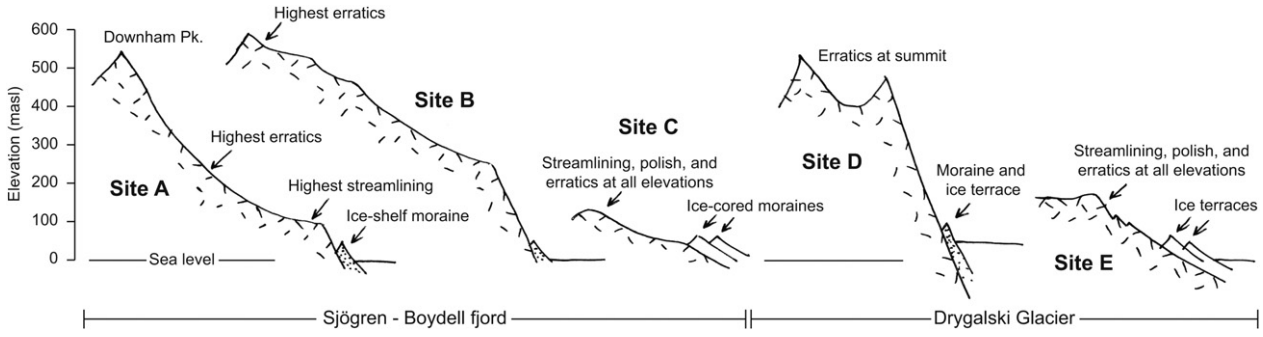

Fig. 2. Sketch showing topography and significant glacial–geologic features at sites visited on NBP10-01.

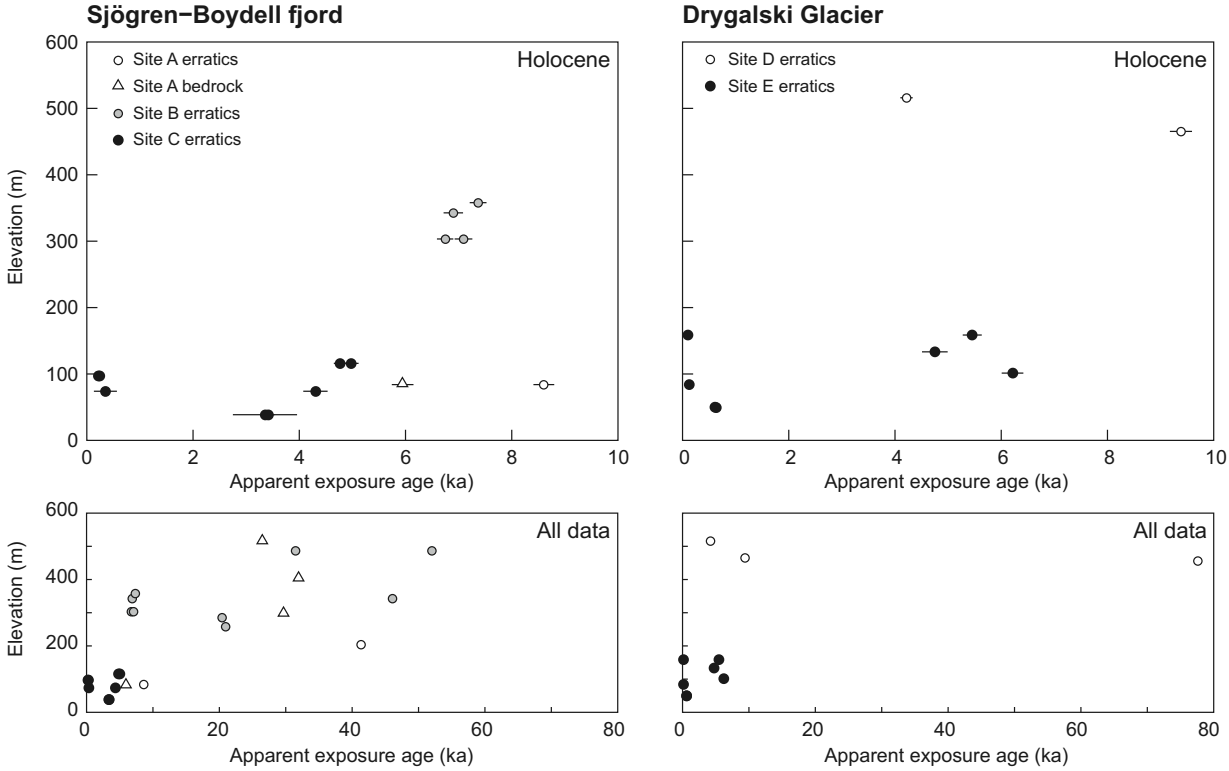

Fig. 3. Apparent ^{10}Be exposure ages from the Sjögren–Boydell fjord and the Drygalski Glacier (also see Table 1). An apparent exposure age is the exposure age calculated from a measured ^{10}Be concentration under the assumption that the sample has experienced a single period of exposure without erosion at its present location. Lower panels show all results; upper panels show only Holocene exposure ages (see text for discussion). Error bars in the upper panels show 1σ internal uncertainties (*sensu* Balco et al., 2008). Where not visible, they are smaller than the symbol size at this scale. Error bars are not shown in the lower panels.

exposure ages of 26–32 ka. At Antarctic sites that were demonstrably covered by LGM ice but also display geomorphic evidence for frozen-based ice cover, it is common to find both bedrock and erratics with apparent exposure ages that greatly predate the LGM (e.g., Sugden et al., 2005). These erratics were deposited during previous interglaciations, but were not removed during periods of ice cover, so their apparent exposure age integrates exposure during multiple ice-free periods. On the other hand, it is unusual to observe bedrock samples with younger apparent exposure ages than those of erratics at similar elevations. As these bedrock samples were collected from upstanding outcrops of friable metasediments that displayed evidence of frost-shattering, we interpret this relationship simply to indicate that upstanding outcrops of foliated, friable bedrock are disintegrating faster than competent granite erratics at this site.

To summarize, observations above 85 m at this site provide no information about the chronology of the most recent deglaciation, but are consistent with the hypothesis that much of this site was covered by frozen-based ice during the LGM. We interpret Holocene ages from both streamlined bedrock and erratics at 80–85 m elevation to show that LGM ice cover was thick enough at some time to support a basal temperature above freezing. The fact that glacier ice was thick enough to support a melted bed at 85 m elevation provides some information on past ice thickness. The thickness of ice required to support basal melting depends on surface climate, flow dynamics, and the geothermal heat flux; simple approximations for glacier thermal structure (e.g., Cuffey and Patterson, 2010) with speculative estimates of LGM surface temperature and geothermal heat flux in this region suggest at least 200–400 m. Thus, it is possible that Downham Peak was entirely ice-covered at the LGM, and none of our observations provide an upper limit on the thickness of LGM ice. The only deglaciation chronology that can be obtained from this site is the exposure ages at 80–85 m elevation, which imply that the ice surface lay at this elevation 8.6–6 ka. This scenario would be consistent with the presence of a PGC ice shelf in the early Holocene.

4.1.2. *Inner fjord, south side (site B)*

This site is a bedrock ridge. At its base (near 250 m elevation) a precipitous slope drops to the fjord; its summit is a peak rising to 595 m elevation (Fig. 2). We examined the ridge between these elevation limits. As at Downham Peak, the surface is nearly completely covered by felsenmeer and colluvium derived from fissile metasedimentary bedrock. We did not observe any striated bedrock or other evidence of subglacial erosion. Glacially transported clasts are rare, but more common than at Downham Peak, and we found them up to 575 m elevation. Of these, many lay in frost cracks or embedded in colluvium; nine were perched on bedrock or felsenmeer and met our criteria for sample collection. Their apparent exposure ages fall into two populations: a set of tightly grouped ages between 6.7 and 7.4 ka at three separate locations between 300 and 360 m elevation; and a set of much older ages, scattered between 20 and 50 ka, at several sites between 260 and 490 m elevation (Table 1; Fig. 3).

The presence of erratics atop apparently undisturbed surficial deposits, combined with the combination of a tightly grouped array of Holocene ages and a scatter of much older ages, is characteristic of Antarctic sites that were covered by frozen-based ice. The distribution of erratics shows that this site was ice-covered to at least 575 m elevation at some time. We interpret the exposure-age data as follows: the older ages provide no information on the most recent deglaciation and, provide only lower limits on the ages of

prior deglaciations; Holocene exposure ages that agree among several sites at similar elevation indicate that the ice surface elevation at this site lay near 300–350 m elevation at 6.5–7.5 ka.

4.1.3. Inner fjord, north side (site C)

This site is a small nunatak adjacent to the calving margin of the Boydell Glacier (Figs. 1, 2 and 4). Its summit lies at 120 m elevation and the ice-free area extends down to present sea level. The surface at this site consists of coarsely streamlined bedrock (schist and gneiss) showing polish, striations, and plucking. Bedrock is overlain by a discontinuous till blanket that includes both local and erratic lithologies. Bedrock and till appear unweathered and fine-grained material in the till has not been removed by deflation. These characteristics indicate that this site was covered by wet-based,

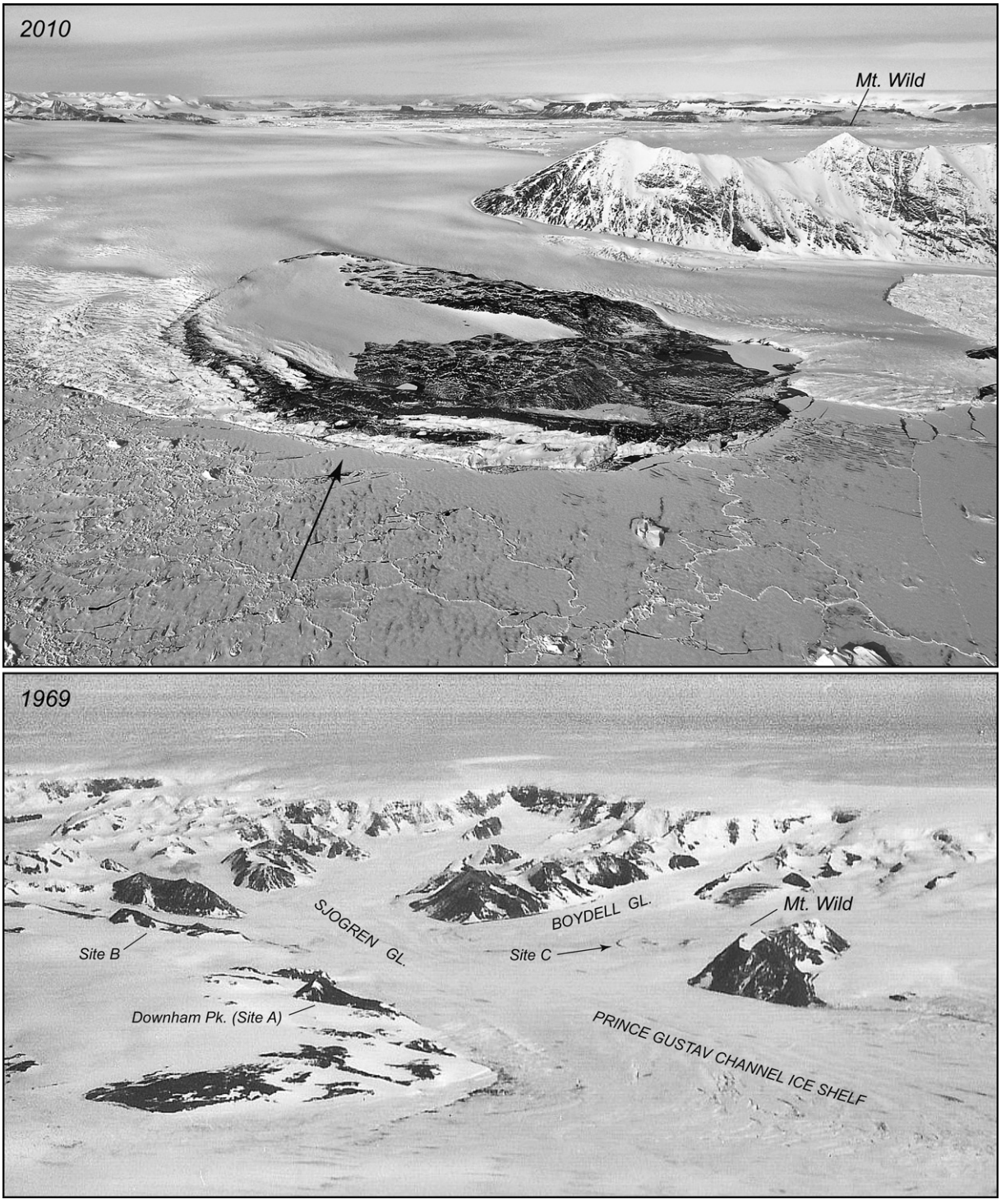

Fig. 4. Aerial photos of unnamed nunatak (site "C") near the margin of the Boydell Glacier in 2010 and 1969. The 2010 image (upper panel) was taken from a helicopter overflying the center of Sjögren–Boydell fjord and looks north over a piedmont glacier to central Prince Gustav Channel. Part of JRI is visible in right background. The 1969 image (lower panel; U. S. Navy photo TMA2159-113R) shows the entire Sjögren–Boydell glacier system and the former PGC ice shelf, viewed from south of JRI looking west toward the Peninsula. The summit plateau and the west side of the Peninsula are obscured by cloud. Mt Wild, a prominent nunatak adjacent to site C, is indicated in both panels. The arrows in both panels point to the same moraine system that rims the west side of the nunatak. Only the uppermost part of the ice-free area that is exposed at present was exposed in 1969.

erosive ice and suggest that deglaciation of the site was recent. Much of this nunatak is bordered by a prominent moraine complex with two major ridges. Although we could not descend the ice-proximal side of this moraine system to measure the ridge elevations accurately, the ice-proximal ridge appears similar in elevation to other moraines and ice terraces that record the 1995 ice shelf surface elevation (De Angelis and Skvarca, 2003). The ice-distal moraine ridge is higher. We examined the ice-distal ridge and found that it consists of only a several-cm-thick surface layer of till, as well as a scatter of larger clasts and boulders, overlying debris-poor glacier ice. Ice pedestals underneath the boulders, precariously balanced boulders, and numerous slumps and gravity-flow deposits in the till layer show that the ice is actively melting. We collected samples from the bedrock part of this nunatak and not the moraine complex.

One important potential issue at this site is that we collected samples as low as 40 m elevation, so we need to consider whether they could have been below sea level at any time. The closest geological evidence for the height of an early Holocene relative sea level highstand that we are aware of is from northeastern JRI, which is variously interpreted to indicate a marine limit at 30 m (Hjort et al., 1997) or 15 m (Roberts et al., 2011). Our sample sites are located closer to the presumed center of an expanded LGM Antarctic Peninsula ice cap, so the marine limit may be higher. We looked for and did not find any evidence of shoreline processes, such as beach ridge formation, erosion or redeposition of till deposits, boulder berm formation by ice shove, or accumulation of rounded clasts, that would indicate submergence. It appears most likely that if the site was below sea level during the early Holocene, it was ice-covered at the time.

Eight exposure ages from this site fall into two groups (Table 1; Fig. 3). First, a group of mid-Holocene exposure ages, including replicate ages at two sites, decrease with elevation from 4.8 ka at 120 m above present sea level to 3.4 ka at 40 m. We interpret this monotonic age–elevation relationship to record mid-Holocene ice surface lowering across the site. Second, a group of samples from intermediate elevations have extremely young apparent exposure ages between 200 and 350 years.

The contrast between these two sets of ages is confusing in several ways. The elevation range of mid-Holocene and very young samples overlap, and in fact at one site samples of similar appearance and geomorphic context, located within meters of one another, have apparent exposure ages of 350 years and 4.4 ka. In addition, a 1969 aerial photo of this site shows that much of the currently-ice-free area of this site, including several of our sample locations, was apparently covered by glacier ice in 1969 (Fig. 4). The moraine complex is visible in its present position on the 1969 photos, but much of the nunatak is covered by permanent snow or ice that appears contiguous with the adjacent glacier, and only our highest two sample sites are visible. We believe the best explanation for these conflicting observations is that the site was fully deglaciated in the mid-Holocene, but was reoccupied by ice sometime before 1969. We hypothesize that late Holocene grounding line advance caused thickening of glaciers adjacent to this site, which was accompanied by partial overrunning of the site by thin marginal ice. As this ice would have been less than 100 m thick, we presume that it would have been frozen-based and would not have disturbed earlier Holocene deposits. This scenario is supported by the 1969 photo showing that the ice or snow covering the nunatak is separated from flowing glacier ice by the moraine complex. Subsequent ablation of that ice could then have deposited a scatter of fresh erratics on top of the array of preexisting erratics that record mid-Holocene deglaciation. This is consistent with the structure of the ice-cored moraines on the south side of the nunatak: as they consist of only a thin skin of debris over an ice core, they could also melt entirely without leaving an obvious or significant debris ridge.

This scenario, even if correct, provides little guidance as to whether we should interpret these young exposure ages as the timing of a glacier advance, the timing of a glacier retreat, or neither. If, as suggested by the historical photos, these samples were exposed by melting between 1969 and 2010, then the apparent exposure ages we observe may reflect residence of the clasts on the ice surface during ablation. In that case they would only provide younger limiting ages for a late Holocene ice advance. Our hypothesis would also imply that the samples with mid-Holocene exposure ages at lower-elevation sites were ice-covered for a time during the late Holocene, in which case their apparent ages would underestimate the age of early Holocene deglaciation. The highest samples from this site, with exposure ages of 4.8 ka, were not covered in 1969 and lie above the level of the ice-cored moraines, so there is no evidence that they were covered during the late Holocene readvance. If they were not covered, then the difference in age between the highest and lowest samples at this site (1.4 ka) is an upper limit on the duration of late Holocene ice cover.

To summarize, the scenario that appears to us most consistent with the exposure ages from this site is that the site was fully deglaciated at 3.5–4.5 ka, that it was partially covered again by thickening of the adjacent Boydell Glacier at or after ca 1.4 ka, and that it was deglaciated again between 1969 and the present.

4.2. Sjögren–Boydell fjord and the Prince Gustav Channel ice shelf: summary

Erratics with Holocene exposure ages up to 360 m elevation at site B show that LGM ice cover reached at least this elevation. The fact that geomorphic evidence for subglacial erosion is present only at low elevation, the presence of erratics atop apparently undisturbed felsenmeer and locally derived colluvium at higher elevations, and the contrast between tightly grouped Holocene exposure ages and scattered older ages, are all consistent with the idea that LGM ice cover in this region was frozen-based at all times above 80–120 m elevation. Evidence for wet-based glaciation at elevations up to 120 m further implies that the LGM ice surface reached at least several hundred meters above this level. Thus, it appears most likely that all the sites we visited were entirely covered by ice during the LGM. However, none of our observations constrain the maximum thickness of LGM ice cover or the time at which this thickness was attained.

We interpret tightly grouped Holocene exposure ages at sites B and C, an internally consistent and replicable age-elevation array of exposure ages at site C, and two Holocene ages from Downham Peak (site A), to indicate ice surface lowering from 350 m elevation (at site B) to near present sea level between 7 ka and 3.5–4.5 ka (Fig. 3). If in fact site C was exposed to present sea level, this would presumably imply the absence of an ice shelf in the Sjögren–Boydell fjord. The coexistence of samples with mid-Holocene exposure ages and those with apparent exposure ages of 200–350 years at a low-elevation site is confusing, but appears best explained by: i) complete deglaciation of the site at 3.5–4.5 ka; ii) glacier advance over the site at or after ca 1.4 ka; and iii) deglaciation in recent decades. This would be consistent with the conclusions of Pudsey and Evans (2001), drawn from marine sedimentary records, that the Prince Gustav Channel ice shelf was absent 5–2 ka and subsequently reformed.

4.3. Drygalski Glacier and the Larsen A ice shelf: site details

The Drygalski Glacier flows into the Larsen A embayment, which was occupied by an ice shelf until its breakup in 1995. Like the

Sjögren and Boydell glaciers, it experienced rapid acceleration and thinning in the years following ice shelf breakup (De Angelis and Skvarca, 2003). We visited two sites near the present calving margin of the Drygalski Glacier: a prominent nunatak near the southern end of the margin called Sentinel Nunatak (Fig. 1, site D), and an unnamed low-elevation rock bench near the northern end of the margin (site E).

4.3.1. Sentinel Nunatak (site D)

The north side of this nunatak is a sheer cliff that drops from 500 m elevation to the glacier; near the bottom of the cliff there are several fragmentary moraines and ice terraces that presumably represent the pre-1995 glacier surface elevation. The south side is less steep and consists of a series of relatively gently sloping west-facing cirques (Fig. 2). We could access elevations between 460 m and the summit at 550 m. The ice-free area at this site is predominantly covered by colluvium and felsenmeer derived from locally outcropping granite and metasedimentary bedrock. We did not observe any geomorphic evidence for subglacial erosion at this site. Numerous erratics within and upon bedrock, felsenmeer, and colluvium indicate that the summit was entirely ice-covered at some point. As at the Sjögren–Boydell fjord sites, the presence of erratics without any geomorphic evidence of subglacial erosion indicates that ice covering Sentinel Nunatak was always frozen-based.

Three erratics from this site had exposure ages of 4.2, 9.4, and 77 ka (Fig. 3). Again, the occurrence of erratics with Holocene exposure ages together with those with much older apparent ages implies that frozen-based ice preserved erratics deposited during pre-LGM deglaciations. The two Holocene ages appear to show that this site was covered by LGM ice and deglaciated during the Holocene. However, the inconsistency in apparent age between these samples implies either that the erratic with the older (9.4 ka) exposure age was emplaced with an inherited nuclide concentration, or that the erratic with the younger (4.2 ka) exposure age was disturbed or covered after emplacement. We found this younger sample perched on felsenmeer within a few meters of an exposed ridgeline, which appeared to us unlikely to have been covered by permanent snow after deglaciation of the site. However, a 1968 aerial photo of the site showed a snowfield or cornice covering this site (Fig. 5). The site of the 9.4 ka exposure age was snow-free in both 1968 and 2010. Thus, we view this age as more reliable. To summarize, we interpret these observations to indicate that the ice surface elevation was most likely near 470 m above present sea level at this site at 9.4 ka.

4.3.2. North side of calving margin (site E)

This site is a terraced bedrock bench whose summit is 160 m above present sea level. Elevations below 50 m are covered by snow and ice at present. In addition, examination of 1968 aerial photos appears to show that the surface of the former Larsen A ice shelf extended well above the lower boundary of the area that is ice-free now. Although the quality of the air photos is not adequate to precisely determine the relative elevations of our sites and the 1968

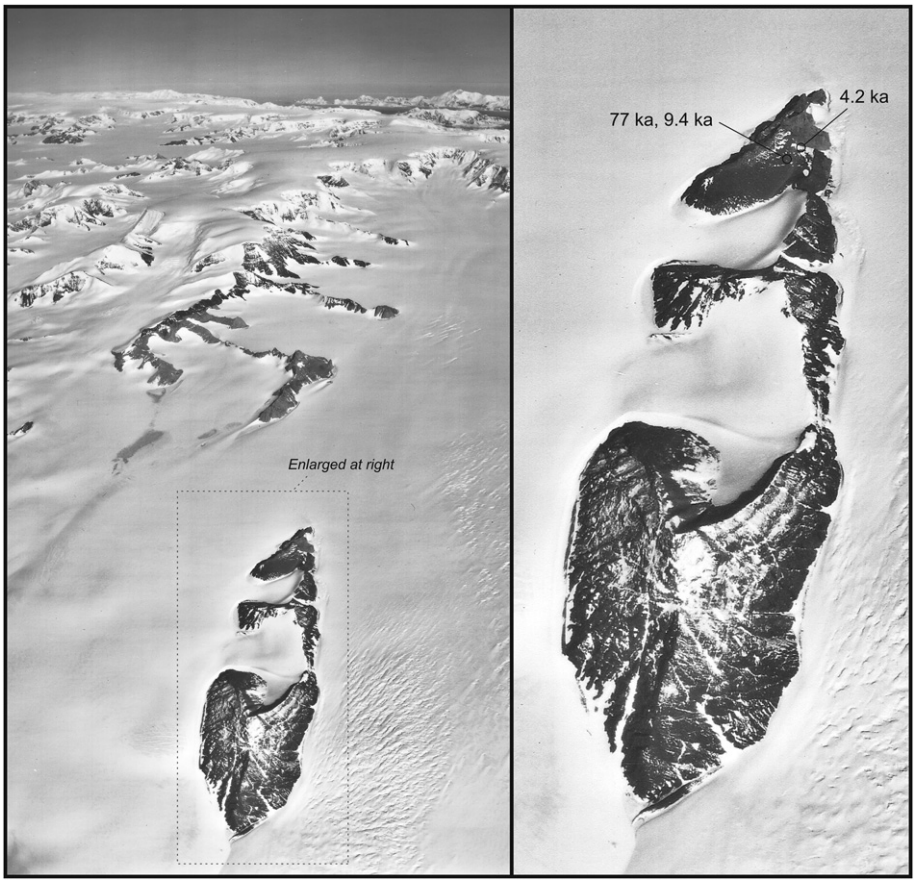

Fig. 5. 1968 aerial photograph of Sentinel Nunatak (U.S. Navy photo TMA2143-312R). View is from the former Larsen A ice shelf near the present calving margin of Drygalski Glacier, looking west up the south side of Drygalski Glacier toward the central plateau of the Peninsula. Open water on the west side of the Peninsula is visible in the distance. Sentinel Nunatak is the prominent nunatak in the foreground that forms the edge of the glacier. The locations of three exposure-dating samples collected from this nunatak are shown in the enlargement at right. The sample with the 4.2 ka exposure age was collected from a sharp ridgeline that was snow-free at the time of collection in 2010, but appears to be covered by a snowfield in 1968. The sample with the 9.4 ka exposure age is snow-free in both cases.

ice surface, it is clear that one or more of our lowest-elevation sample sites were ice-covered in 1968. Bedrock at this site is foliated schist-to-gneiss-grade metasediments. The surface consists nearly entirely of coarsely streamlined bedrock, and striations are evident on many upstanding bedrock knobs; this indicates that this site was covered by wet-based and erosive ice. Erratics, stones of local lithology but with evidence of subglacial transport, and discontinuous till patches occur throughout the site, although till patches are more common at lower elevations. Seven samples from this site yielded results similar to those we observed at site C in the Sjögren–Boydell fjord: a bimodal distribution of samples with mid-Holocene apparent exposure ages of 4.8–6.2 ka coexisting with samples having very young apparent exposure ages of 100–600 years (Fig. 3). In contrast to site C, however, the age–elevation relationship of the mid-Holocene data is scattered.

We interpret these observations to be best explained by the same scenario that we proposed above for site C: the erratics with exposure ages of 4.7–6.2 ka record middle Holocene deglaciation of this site, and the very young exposure ages record glacier or ice shelf thickening that caused thin marginal ice from a thicker Drygalski Glacier or Larsen A ice shelf to spill over onto the site during the late Holocene. However, even if our hypothesis is correct, the fact that both mid-Holocene and very recent exposure ages occur at all elevations and show scattered age–elevation relationships precludes a meaningful estimate of the duration of late Holocene ice cover.

4.4. Drygalski Glacier and the Larsen A ice shelf: summary

The exposure-age data from the Drygalski Glacier sites are fewer and more scattered than those from the Sjögren–Boydell fjord sites, but present essentially the same picture.

The presence of erratics with Holocene exposure ages to 520 m indicates that the LGM ice surface lay at or above this elevation. The fact that these erratics overlie undisturbed felsenmeer and colluvium indicates frozen-based ice at this elevation. Again, these data do not constrain the maximum LGM ice thickness or the time that it may have occurred. At low-elevation sites, evidence for subglacial erosion as well as Holocene exposure ages show that LGM ice was wet-based at and below 160 m elevation, and appear to indicate that the ice surface elevation was near 100–150 m at 4.5–6.5 ka.

We interpret the bimodal distribution of erratics with exposure ages of only a few hundred years and those with mid-Holocene exposure ages to be best explained by glacier or ice shelf thickening and encroachment of marginal ice near or over the site. The ice-free period started no later than 4.8–6.2 ka, but could have started earlier; the data do not constrain when it may have ended. This scenario is consistent with the observations of Brachfeld et al. (2003) that the Larsen A ice shelf was absent 3.8–1.4 ka.

5. Conclusions

Cosmogenic-nuclide exposure ages of glacial erratics, collected from a range of elevations at currently ice-free areas of the northeast Antarctic Peninsula, provide a record of Holocene glacier and ice shelf change.

Glacial-geologic observations and erratics with Holocene exposure ages show that the LGM ice sheet surface near the present coastline was locally at least 520 m above present relative sea level. LGM ice was always frozen-based at elevations above 100–150 m. None of our observations constrain the maximum thickness of LGM ice or the time at which it was attained.

Ice surface lowering, from at least 520 m above present sea level at the modern coastline to near present sea level, took place between 9.4 ka and 4.5–3.5 ka. We do not have enough data to resolve differences in the timing of glacier thinning between the Sjögren–Boydell and Drygalski Glaciers, nor to evaluate the hypothesis that deglaciation may have occurred by a series of rapid grounding line retreats punctuated by periods of relative stability.

At two sites near present glacier margins and below 100–150 m elevation, apparent exposure ages of erratics show a bimodal distribution, with a population of mid-Holocene apparent exposure ages coexisting with one having apparent exposure ages of 100–600 years. Historical aerial photography shows that many of these erratics with very young exposure ages were most likely exposed in the last 40 years, possibly by glacier thinning after ice shelf breakup in 1995. We interpret these observations to be best explained by: i) complete deglaciation of the currently ice-free areas, which presumably required the absence of ice shelves, at 3.5–4.5 ka, followed by ii) subsequent ice shelf formation, grounding line advance, glacier thickening, and expansion of frozen-based ice over our sample sites during the late Holocene, most likely after 1.4 ka, and iii) complete re-exposure of these sites after recent ice shelf breakup and glacier surface lowering. These observations are consistent with marine sedimentary records indicating that ice shelves in the Prince Gustav Channel and Larsen A embayment were absent in the middle to late Holocene and were re-established within the last 2000 years.

Acknowledgments

This work could not have been accomplished without the skill and hard work of the following individuals: Captain Joe Borkowski and the crew of the *Nathaniel B. Palmer*; Chris Dean, Barry James, Randy Perrodin, and Jay Cox of PHI, Inc.; and the NBP10-01 shipboard science party. Dylan Rood was instrumental in carrying out the AMS analyses. This work is a part of the "LARISSA" project and was funded by the U.S. National Science Foundation under grant ANT-0732467 to Hamilton College. This is LDEO contribution 7625. GB thanks Rob Larter of the British Antarctic Survey for providing the gridded bathymetric data shown in Fig. 1. The staff of the U.S. Antarctic Resource Center assisted in locating historical air photography. Joanne Johnson and Bethan Davies provided helpful and comprehensive reviews. Finally, GB greatly appreciates the forbearance and good humor of pilot Barry James and reporter Doug Fox during an unscheduled three-day stop on James Ross Island.

References

Balco, G., Briner, J., Finkel, R., Rayburn, J., Ridge, J., Schaefer, J., 2009. Regional beryllium-10 production rate calibration for late-glacial northeastern North America. Quaternary Geochronology 4, 93–107.

Balco, G., Stone, J., Lifton, N., Dunai, T., 2008. A complete and easily accessible means of calculating surface exposure ages or erosion rates from ^{10}Be and ^{26}Al measurements. Quaternary Geochronology 3, 174–195.

Bentley, M., Fogwill, C., Le Brocq, A., Hubbard, A., Sugden, D., Dunai, T., Freeman, S., 2010. Deglacial history of the West Antarctic Ice Sheet in the Weddell Sea embayment: constraints on past ice volume change. Geology 38, 411–414.

Brachfeld, S., Domack, E., Kissel, C., Laj, C., Leventer, A., Ishman, S., Gilbert, R., Camerlenghi, A.L.E., 2003. Holocene history of the Larsen-A ice shelf constrained by geomagnetic paleointensity dating. Geology 31, 749–752.

Cook, A., Vaughan, D., 2010. Overview of areal changes of the ice shelves on the Antarctic Peninsula over the past 50 years. The Cryosphere 4, 77–98.

Cuffey, K., Conway, H., Gades, A., Hallet, B., Lorain, R., Severinghaus, J., Steig, E., Vaughn, B., White, J., 2000. Entrainment at cold glacier beds. Geology 28 (4), 351–354.

Cuffey, K., Patterson, W., 2010. The Physics of Glaciers, fourth ed. Academic Press.

Davies, B., Hambrey, M., Smellie, J., Carrivick, J., Glasser, N., 2012. Antarctic Peninsula Ice Sheet evolution during the Cenozoic Era. Quaternary Science Reviews 31, 30–66.

De Angelis, H., Skvarca, P., 2003. Glacier surge after ice shelf collapse. Science 299, 1560–1562.

Domack, E., Duran, D., Leventer, A., Ishman, S., Doane, S., McCallum, S., Amblas, D., Ring, G., Gilbert, R., Prentice, M., 2005. Stability of the Larsen B ice shelf on the Antarctic Peninsula during the Holocene epoch. Nature 436, 681–685.

Evans, J., Pudsey, C., ÓCofaigh, C., Morris, P., Domack, E., 2005. Late Quaternary glacial history, flow dynamics, and sedimentation along the eastern margin of the Antarctic Peninsula Ice Sheet. Quaternary Science Reviews 24, 741–774.

Heroy, D., Anderson, J., 2007. Radiocarbon constraints on Antarctic Peninsula Ice Sheet retreat following the Last Glacial Maximum (LGM). Quaternary Science Reviews 26, 3286–3297.

Hjort, C., Bjorck, S., Ingolfsson, O., Moller, P., 1998. Holocene deglaciation and climate history of the northern Antarctic Peninsula region: a discussion of correlations between the Southern and Northern Hemispheres. Annals of Glaciology 27, 110–112.

Hjort, C., Ingolfsson, O., Moller, P., Lirio, J., 1997. Holocene glacial history and sea-level changes on James Ross Island, Antarctic Peninsula. Journal of Quaternary Science 12 (4), 259–273.

Ingolfsson, O., Hjort, C., Bjorck, S., Smith, R., 1992. Late Pleistocene and Holocene glacial history of James Ross Island, Antarctic Peninsula. Boreas 21 (3), 209–222.

Johnson, J., Bentley, M., Roberts, S., Binnie, S., Freeman, S., 2011. Holocene deglacial history of the northeast Antarctic Peninsula: a review and new chronological constraints. Quaternary Science Reviews 30, 3791–3802.

Kaplan, M.R., Strelin, J.A., Schaefer, J.M., Denton, G.H., Finkel, R.C., Schwartz, R., Putnam, A.E., Vandergoes, M.J., Goehring, B.M., Travis, S.G., 2011. In-situ cosmogenic ^{10}Be production rate at Lago Argentino, Patagonia: implications for late-glacial climate chronology. Earth and Planetary Science Letters 309 (1–2), 21–32.

Liu, H., Jezek, B., Zhao, Z., 2001. Radarsat Antarctic Mapping Project Digital Elevation Model, Version 2. Technical Report. National Snow and Ice Data Center, Boulder, CO, USA.

Nishiizumi, K., Imamura, M., Caffee, M., Southon, J., Finkel, R., McAnich, J., 2007. Absolute calibration of ^{10}Be AMS standards. Nuclear Instruments and Methods in Physics Research B 258, 403–413.

Pudsey, C., Evans, J., 2001. First survey of Antarctic sub-ice shelf sediments reveals mid-Holocene ice shelf retreat. Geology 29, 787–790.

Putnam, A., Schaefer, J., Barrell, D., Vandergoes, M., Denton, G., Kaplan, M., Finkel, R., Schwartz, R., Goehring, B., Kelley, S., 2010. In situ cosmogenic ^{10}Be production-rate calibration from the Southern Alps, New Zealand. Quaternary Geochronology 5, 392–409.

Roberts, S., Hodgson, D., Sterken, M., Whitehouse, P., Verleyen, E., Vyverman, W., Sabbe, K., Balbo, A., Bentley, M., Moreton, S., 2011. Geological constraints on glacio-isostatic adjustment models of relative sea-level change during deglaciation of Prince Gustav Channel, Antarctic Peninsula. Quaternary Science Reviews 30, 3603–3617.

Rott, H., Skvarca, P., Nagler, T., 1996. Rapid collapse of northern Larsen Ice Shelf, Antarctica. Science 271 (5250), 788–792.

Scambos, T., Bohlander, J., Shuman, C., Skvarca, P., 2004. Glacier acceleration and thinning after ice shelf collapse in the Larsen B embayment, Antarctica. Geophysical Research Letters 31 (18).

Stone, J., Balco, G., Sugden, D., Caffee, M., Sass III, L., Cowdery, S., Siddoway, C., 2003. Holocene deglaciation of Marie Byrd Land, West Antarctica. Science 299, 99–102.

Strelin, J., Sone, T., Mori, J., Torielli, C., Nakamura, T., 2006. New data related to Holocene landform development and climatic change from James Ross Island, Antarctic Peninsula. In: Fütterer, D., Damaske, D., Kleinschmidt, G., Miller, H., Tessensohn, F. (Eds.), Antarctica: Contributions to Global Earth Sciences. Springer-Verlag, pp. 455–460.

Sugden, D., Balco, G., Cowdery, S., Stone, J., Sass III, L., 2005. Selective glacial erosion and weathering zones in the coastal mountains of Marie Byrd Land, Antarctica. Geomorphology 67, 317–334.

Todd, C., Stone, J., Conway, H., Hall, B., Bromley, G., 2010. Late Quaternary evolution of Reedy Glacier, Antarctica. Quaternary Science Reviews 29, 1328–1341.

Vaughan, D., Doake, C., 1996. Recent atmospheric warming and retreat of ice shelves on the Antarctic Peninsula. Nature 379 (6563), 328–331.